nature energy

ARTICLES

https://doi.org/10.1038/s41560-021-00848-z

Low-temperature and effective ex situ group V doping for efficient polycrystalline CdSeTe solar cells

Deng-Bing Li[1], Canglang Yao[1], S. N. Vijayaraghavan[2], Rasha A. Awni[1], Kamala K. Subedi[1], Randy J. Ellingson[1], Lin Li[2], Yanfa Yan[1]✉ and Feng Yan[2]✉

CdTe solar cell technology is one of the lowest-cost methods of generating electricity in the solar industry, benefiting from fast CdTe absorber deposition, $CdCl_2$ treatment and Cu doping. However, Cu doping has low photovoltage and issues with instability. Doping group V elements into CdTe is therefore a promising route to address these challenges. Although high-temperature in situ group V doped CdSeTe devices have demonstrated efficiencies exceeding 20%, they face obstacles including post-deposition doping activation processes, short carrier lifetimes and low activation ratios. Here, we demonstrate low-temperature and effective ex situ group V doping for CdSeTe solar cells using group V chlorides. For $AsCl_3$ doped CdSeTe solar cells, the dopant activation ratio can be 5.88%, hole densities reach $>2\times10^{15}$ cm^{-3} and carrier lifetime is longer than 20 ns. Thus, ex situ As doped CdSeTe solar cells show open-circuit voltages ~863 mV, compared to the highest open-circuit voltage of 852 mV for Cu doped CdSeTe solar cells.

The polycrystalline CdTe photovoltaic (PV) device is one of the most successful commercial thin-film solar cell technologies, with a record power conversion efficiency (PCE) of over 22%, a module that is cost competitive with Si modules and more than 25 GW worth of solar modules installed worldwide[1–4]. So far, all manufacturing processes of CdTe-based PV modules include three critical steps at different temperatures: fast absorber (CdTe or CdSe/CdTe) deposition (~600 °C), $CdCl_2$ treatment (~400 °C) and Cu doping (~200 °C)[5,6]. The ex situ diffusion Cu doping introduces hole carriers in the absorber layers, which are needed for efficient CdTe solar cells. However, Cu doping possesses two major shortfalls that limit the performance of current CdTe-based PV modules. First, due to defect compensation, Cu doping is only able to produce a low hole density of ~10^{14} cm^{-3}, which is about two orders of magnitude lower than the optimum hole density (~10^{16} cm^{-3}) needed to maximize the PCE of CdTe-based PV modules[7]. Second, Cu ions easily migrate and diffuse spatially, creating a risk of module instabilities[8].

For many decades, lots of effort has been expended to address these shortfalls of Cu doping by exploring other dopants, especially group V doping via substitutional incorporation of elements such as phosphorus, arsenic, antimony and bismuth (Supplementary Table 1 shows the various group V doping approaches in CdTe-based solar cells). Theoretical studies have predicted that group V doping is capable of overcoming the two shortfalls of Cu doping[9,10]. Both in situ and ex situ group V doping have been explored experimentally. The US National Renewable Energy Laboratory (NREL) and First Solar Inc. have demonstrated a high hole density of 1×10^{17} cm^{-3} and a PCE of 20% with excellent device stability through in situ group V doping[5], showing the method's impressive capability to overcome the shortfalls of Cu doping in CdTe-based solar cells. Other in situ group V doping approaches include providing Cd_3V_2 powders (where V is a group V element) dope in single-crystal CdTe growth[11], tris-dimethylaminoarsine in metal–organic chemical vapour deposition growth[12] and arsine (AsH_3) in polycrystalline CdTe-based thin films[13]. However, most of these in situ group V doping techniques require complex annealing processes to activate the dopants[5]. In addition, high deposition temperatures such as those used in vapour transport deposition (VTD) are thermodynamically favourable to the formation of Cd-deficient CdTe films[10], making it energetically unfavourable to dope As at Te sites (As_{Te}). Providing additional Cd vapour is an effective way to mitigate this problem during group V doping in CdTe single crystals[14]. However, neither high-temperature (>1,000 °C) annealing of CdTe single crystals in sealed quartz ampoules nor special high-temperature post-deposition activation is compatible with current industry technology[2]. Nonetheless, the dopant activation ratio, which is defined as the hole density relative to an incorporated dopant quantity, is only about 1.5% in VTD As doped polycrystalline CdTe-based absorbers due to complicated compensation processes[15]. Additionally, in situ group V doping introduces a uniform distribution of dopants in the CdTe absorber layer[5], impeding desirable dopant depth profiles[16,17].

A low-temperature ex situ diffusion of group V dopants is preferred and fully compatible with mainstream CdTe-based solar module fabrication. Importantly, ex situ group V doping can be performed in chlorinated CdTe (that is, $CdCl_2$-treated CdTe)[18], which is more desirable for the formation of substantial group V on Te sites (V_{Te}). Although group V diffusion doping in CdTe and the desirable depth profiles have been successfully demonstrated[19], high efficiency CdTe solar cells using ex situ group V doping have proved elusive (Supplementary Table 1). Reported ex situ group V doping approaches include annealing CdTe in group V vapour[20], group V ion implantation[21] and depositing a group V Te back buffer layer followed by thermal diffusion[22]. For instance, using Sb_2Te_3 as back contact produced a PCE of 13.1% with an open-circuit voltage (V_{OC}) of 816 mV after annealing at 300 °C (ref. [23]). However,

[1]Department of Physics and Astronomy and Wright Center for Photovoltaics Innovation and Commercialization, University of Toledo, Toledo, OH, USA. [2]Department of Metallurgical and Materials Engineering, The University of Alabama, Tuscaloosa, AL, USA. ✉e-mail: yanfa.yan@utoledo.edu; fyan@eng.ua.edu

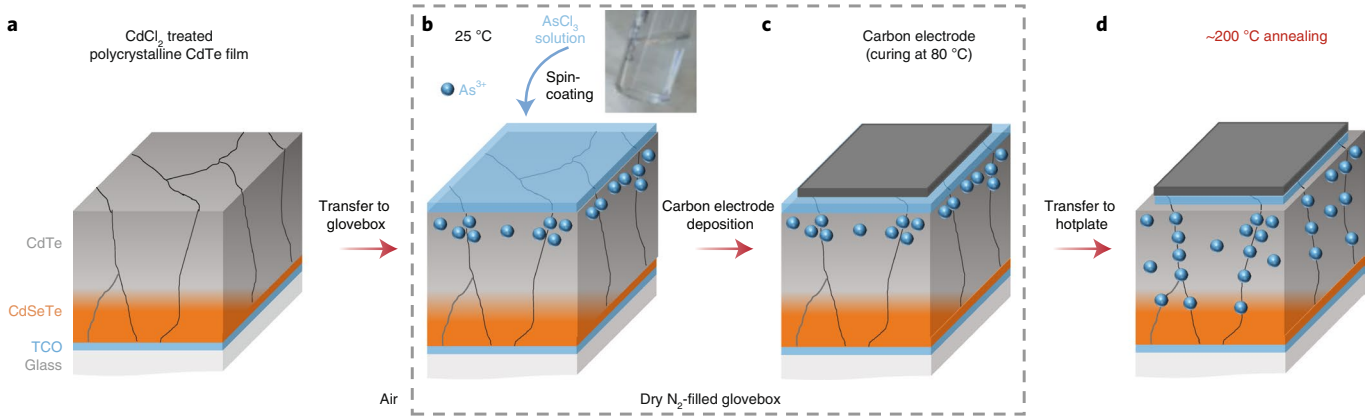

Fig. 1 | Schematic of low-temperature ex situ doping in polycrystalline CdSeTe solar cells. a, $CdCl_2$-treated polycrystalline CdSeTe films. **b**, Solution-processed group V deposition using the group V chlorides VCl_3 (that is, PCl_3, $AsCl_3$, $SbCl_3$ and $BiCl_3$) solution on the CdSeTe surface. Here, $AsCl_3$ was chosen as an example. A photograph of the transparent, colourless $AsCl_3$ solution is shown in the inset. All the other VCl_3 solutions had similar appearances. **c**, Low-temperature carbon electrode was applied to the VCl_3 coated CdSeTe film and was cured to dry at 80 °C. The steps shown in **b** and **c** are both processed in the dry N_2-filled glovebox to prevent the hydrolysis of VCl_3 and/or due to its toxicity. **d**, Group V diffusion into CdSeTe at low temperature (~200 °C) with carbon electrode.

the residual Sb_2Te_3 creates a large hole transport barrier (0.4 eV) at the CdTe/Sb_2Te_3 interface due to the defect compensation, which limits further improvement of the PCE[23]. Also, the similarity of the Pauling electronegativity of group V elements to those of Te and Cd (Supplementary Table 2) indicates that V–Te and Cd–V bonds have highly covalent characteristics, suggesting that higher energy is required to break the covalent bond before the group V element can diffuse into CdTe. Therefore, a higher annealing temperature is required to facilitate the diffusion of group V elements.

Here, a series of group V highly ionic materials (that is, group V chlorides (VCl_3) such as PCl_3, $AsCl_3$, $SbCl_3$ and $BiCl_3$) are used as dopant precursors in a solution method (Supplementary Table 3) with various physical properties differing from those of Cd group V compounds (that is, Cd_3V_2 compounds such as Cd_3P_2 and Cd_3As_2), enabling low-temperature and effective ex situ group V doping in polycrystalline CdTe thin-film solar cells. Density functional theory (DFT) calculations, materials synthesis and characterizations and device fabrication and measurements are used to validate this strategy. For $AsCl_3$ ex situ doped CdSeTe films, we achieved hole densities $>2\times10^{15}\,cm^{-3}$ and carrier lifetimes longer than 20 ns. As a result, our ex situ group V doped CdSeTe solar cells achieve a V_{OC} as high as 863 mV, compared with the highest V_{OC} of 852 mV for Cu doped solar cells. These results demonstrate success in fabricating polycrystalline CdSeTe solar cells doped by group V elements using an ex situ and low-cost process that is completely compatible with current industrial manufacturing lines, opening a new direction for research on group V doped polycrystalline CdTe-based thin-film solar cells.

Problem and mitigation strategy for ex situ group V doping. As described above, the need for annealing temperatures exceeding 600 °C for previous ex situ group V doping using Cd_3As_2 as dopant source is the main reason for the poor performance of CdTe solar cells. However, our DFT calculations suggest that high-temperature annealing may not be essential for effective diffusion of group V dopants in CdTe (Supplementary Table 4 and Supplementary Fig. 1). Previous DFT calculations have shown that the diffusion barriers for group V dopants in CdTe are in the range of 0.4–0.8 eV, depending on the charge state of the group V dopants[20]. Our DFT-calculated diffusion barriers for Cd in CdTe are in the range of 0.35–0.40 eV (Supplementary Table 4 and Supplementary Fig. 1), only slightly smaller than those of group V dopants. Cd atoms readily diffuse at temperatures above 300 °C (ref. [24]). We hypothesize that the reason high annealing temperatures in a sealed ampoule are required could be to provide sufficient vapour pressure of group V elements rather than to overcome the ion diffusion barrier[20].

If our hypothesis is correct, the required annealing temperature may be substantially lowered by depositing appropriate back contact before the diffusion annealing. Inspired by the $CdCl_2$ heat treatment (~400 °C) and doping with Cu chlorides (that is, CuCl and $CuCl_2$; ~200 °C) in CdTe-based solar cells[25–27], we propose to use group V chlorides (for example, PCl_3, $AsCl_3$, $SbCl_3$ and $BiCl_3$) as the group V dopant sources in CdSeTe solar cells, which can also help avoid the loss of Cl during the annealing after $CdCl_2$ treatment[28]. Group V chlorides are salts that can be dissolved in organic solutions, thus allowing room-temperature solution deposition (Supplementary Table 3). The ionic nature of these salts makes diffusion of group V cations easier at low annealing temperatures. However, because of the ready hydrolysis, toxicity or both of VCl_3 compounds, the deposition must be done in an inert environment, such as a dry N_2-filled glovebox. This further implies that the back contact must also be deposited in an inert environment and at room temperature. Therefore, we employ a low-temperature carbon paste as the back contact with a curing temperature <100 °C, which can be deposited by screen printing in the glovebox at room temperature (Supplementary Fig. 2). Note that the carbon electrode is not the best back contact material for CdTe-based solar cells, but it provides a feasible and fast way for us to validate our proposed strategy (Fig. 1).

Ex situ diffusion doping to polycrystalline CdSeTe thin film. In this work, we use $AsCl_3$ as a representative to dope chlorinated CdSeTe films (CdSeTe doped with other group V chloride can be seen in the Supplementary Information). Figure 1 shows the fabrication steps of the low-temperature group V diffusion doping beginning with a chlorinated polycrystalline CdSeTe film (other group VCl_3 doping procedures are shown in Supplementary Fig. 2). The detailed fabrication procedures can be found in Methods. To address the challenges posed by the ready hydrolysis and toxicity of $AsCl_3$, the cleaned and etched CdSeTe films were transferred to a dry N_2-filled glovebox to perform doping treatment. The transparent $AsCl_3$ solution was prepared in the glovebox as shown in the inset of Fig. 1b. $AsCl_3$ diffusion doping was performed in three basic steps. (1) The $AsCl_3$ layer was deposited on the CdSeTe surface at

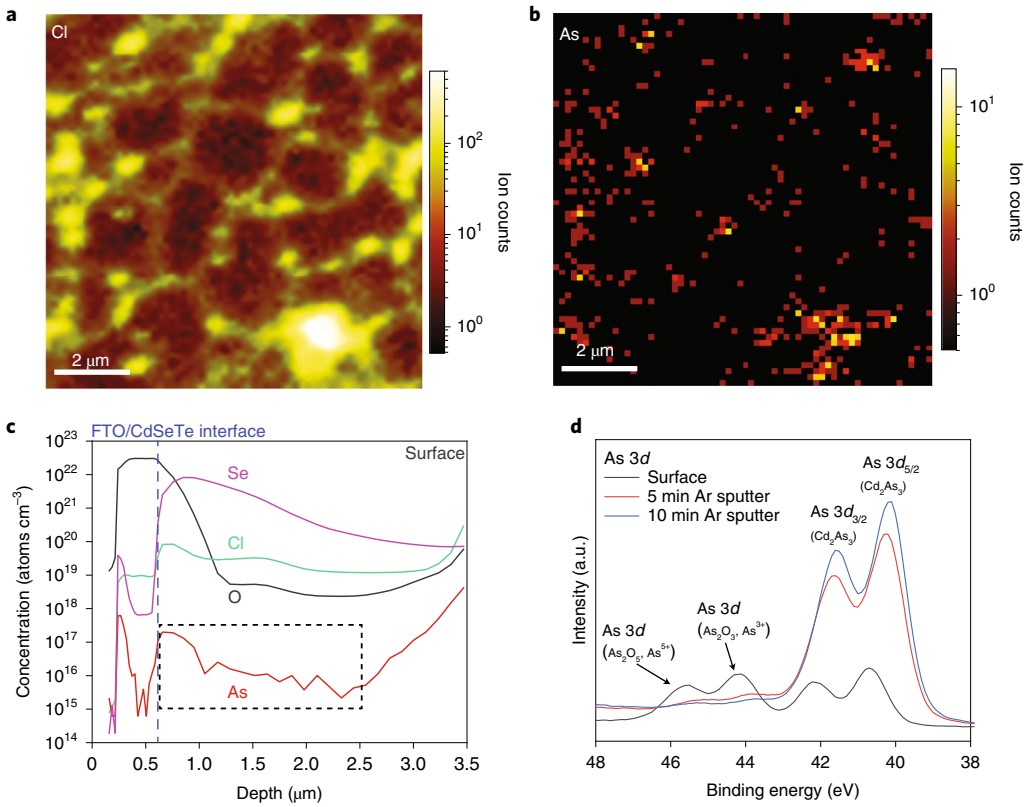

Fig. 2 | Characterizations of dopant distribution and the formation of shallow acceptor states. a, 2D Cl distribution mapping ($10\times10\,\mu m^2$) using ToF-SIMS shows that Cl accumulates at the GBs. **b**, 2D As distribution mapping of the same area shown in **a**. **c**, Dynamic SIMS depth profiles for the As doped CdSeTe device. The dashed line on the SIMS depth profile indicates the location of the fluorine-doped tin oxide (FTO)/CdSeTe interface, and the square indicates the [As] used for activation calculation. **d**, X-ray photoelectron spectroscopy (XPS) analysis of the chemical state of As ions in the As doped CdSeTe before and after 5 min (~5 nm) and 10 min (~10 nm) Ar pre-sputter etching.

room temperature using a spin-coater (Fig. 1b). The dosage of group V dopant is controlled by varying the $AsCl_3$ solution concentration (for example, from 1 to ~100 mg l^{-1}) with a fixed spin-coating rate of 1,000 revolutions per min. (2) Carbon paste was screen-printed on the $AsCl_3$-coated CdSeTe surface followed by curing at 80 °C (Fig. 1c). (3) The devices were transferred out of the glovebox and annealed at ~200 °C for various times to facilitate the diffusion of the As dopants into CdSeTe (Fig. 1d). For comparison, CuCl was selected as a Cu dopant source to fabricate reference devices[25]. Note that the low-cost low-temperature carbon paste is Cu free with a work function of ~5.0 eV (ref. [29]).

To image the As distribution in the polycrystalline CdSeTe films, two-dimensional time-of-flight secondary ion mass spectrometry (2D-ToF-SIMS) mappings and dynamic SIMS depth profiles were collected for the finished devices after annealing at 200 °C. Taking advantage of the segregation of Cl at grain boundaries (GBs) after $CdCl_2$ treatment[18,30], we used 2D-ToF-SIMS mapping of Cl to trace the GBs (Fig. 2a). The 2D-ToF-SIMS mapping of As ions (Fig. 2b) shows the accumulation of As ions at the CdSeTe GBs, which is similar to the ex situ diffusion behaviour of Cu[20,31]. This is because As ions show much higher diffusion constants (D) ($D_{GB,As}$ ~1.05×10^5 cm^2 s^{-1} versus $D_{GI,As}$ ~9.4×10^{-2} cm^2 s^{-1}) and solubility in GBs than grain interiors (GIs) (Supplementary Table 4)[20,31,32]. The GBs act as pathways for fast diffusion of As ions from the back surface to the front of CdSeTe devices, which facilitates the subsequent diffusion from the GBs into the GIs (Fig.1d). Unfortunately, as the ToF-SIMS As detection limit (~1×10^{18} cm^{-3}) is lower than the As concentration ([As]) (<10^{18} cm^{-3}) in the CdSeTe bulk region (Fig. 2c), the 2D-ToF-SIMS mapping is not able to quantify the As distribution at CdSeTe GIs. Therefore, we used 2D dynamic SIMS to examine the As distributions in GIs. 2D dynamic SIMS has a ~100 times better detection limit than 2D-ToF-SIMS, but a lower spatial resolution (~4–5 μm). To enable meaningful 2D dynamic SIMS elemental mapping, we synthesized a 10 μm thick CdSeTe film that has grains as large as 10 μm (Supplementary Fig. 3a) and conducted the same $AsCl_3$ treatment. Supplementary Fig. 3b shows the 2D dynamic SIMS mapping of Cl, which is used as a reference to identify the location of GBs and GIs. Supplementary Figure 3c shows the 2D dynamic SIMS mapping of As, which also shows the accumulation of As at GBs. Supplementary Figure 3d shows the line profiles of As across the GBs. The locations of GBs are marked according to the line profile of Cl. The distribution of As in GIs can be observed, though the average intensity is about three times lower than that in GB regions. We expect that similar diffusivity behaviour of As (that is, from GBs into GIs) also exists in CdSeTe devices with smaller grain sizes.

Benefiting from the ex situ diffusion doping dynamics, the [As] shows a desirable depth profile: [As] is at least two orders of magnitude higher at the surface than in the bulk of CdSeTe (Fig. 2c). At the CdSeTe back surface, the [As] is ~5.8×10^{18} cm^{-3}, which is comparable to the homogeneous [As] in the in situ doped polycrystal CdSeTe (1.0×10^{18} cm^{-3}) (ref. [5]) and the ex situ doped single-crystal CdSeTe (5.5×10^{17} m^{-3}) (ref. [33]). This heavily As doped CdSeTe layer near the back contact can help to form an ohmic back contact and improve the device performance[34]. By contrast, the average [As] in the CdSeTe bulk (between the FTO/CdSeTe front interface and 2 μm away from it) is only ~4.27×10^{16} cm^{-3}, with slight As segregation at the front absorber/buffer interface (Fig. 2c), which is similar to the Cu distribution in efficient Cu doped devices[16,35].

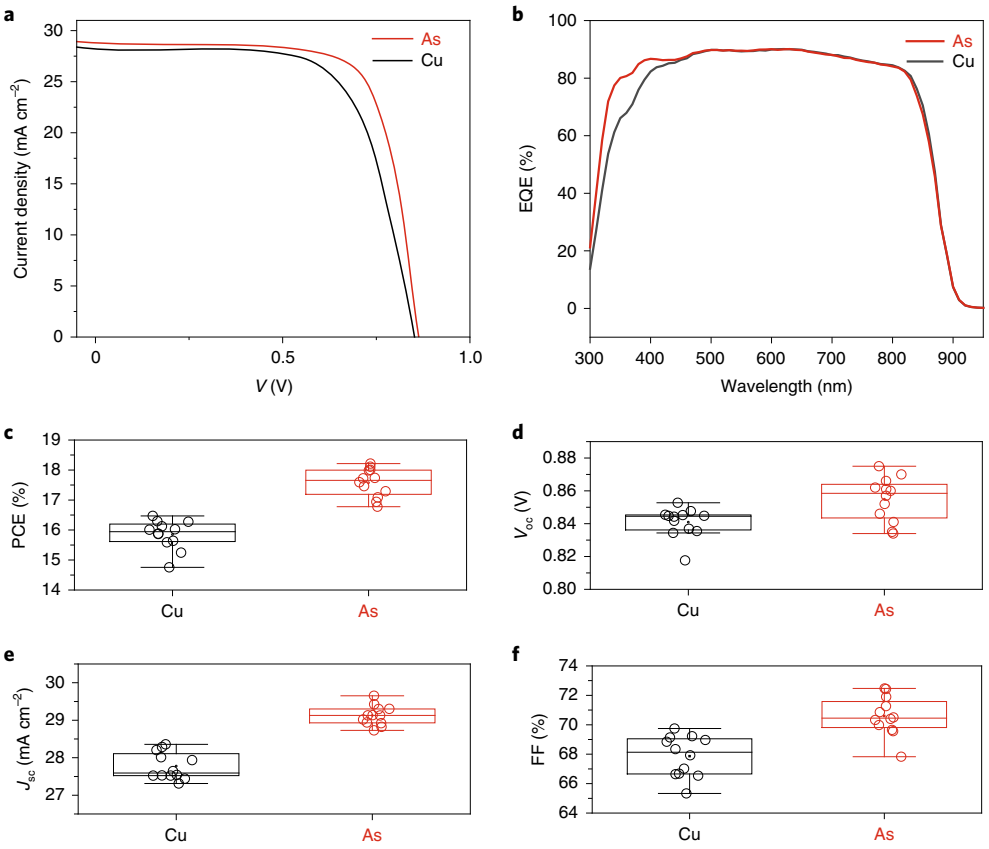

Fig. 3 | Improvement of $AsCl_3$ doped Cu-free CdSeTe device performances. a, *J*–*V* curves for CdSeTe solar cells doped with CuCl or $AsCl_3$. **b**, Corresponding EQE for the CuCl and $AsCl_3$ doped CdSeTe solar cells as a function of wavelength. **c**–**f**, The statistical distribution of the PV parameters (centre line shows the median, box shows the upper and lower quartiles and the whiskers show the full range; each black and red circle in the box and whisker plots presents the value of the *J*–*V* performances for one cell; cell number = 12) of PCE (**c**), V_{OC} (**d**), short-circuit current density (J_{SC}) (**e**), and fill factor (FF; **f**).

XPS was used to characterize the chemical states of the doped group V elements in the CdSeTe (Supplementary Fig. 4 and Supplementary Table 5). The result for the As doped device is shown in Fig. 2d. The surface As was notably oxidized due to exposure to air during the sample transfer. Remarkably, most of the As oxides were removed after ~5–10 nm surface etching by Ar sputter, leaving the pronounced binding energies of As $3d_{5/2}$ at 40.3 eV and $3d_{3/2}$ at 41.8 eV. Both of these binding energies can be assigned to As^{3-} ions in the Cd_3As_2 compound, suggesting the formation of shallow acceptor defects As_{Te}^{-} (ref. [36]). Note that the reduction of As^{3+} ions in $AsCl_3$ to As^{3-} ions takes place once the As^{3+} ions have diffused into the CdSeTe, due to As having a higher Pauling electronegativity than Te (2.18 for As versus 2.10 for Te).

The SIMS and XPS results have demonstrated the diffusion route, elemental distribution and chemical states of As dopants in CdSeTe film. Compared to other ex situ group V doping techniques using Cd_3V_2 or V_2Te_3 compounds as doping sources, our $AsCl_3$ solution treatment possesses two advantages. One is that the ionic radius of As^{3+} in $AsCl_3$ (~0.58 Å) is much smaller than the ionic radius of As^{3-} in Cd_3As_2 (~2.22 Å), which can presumably reduce the diffusion barrier in CdSeTe lattice. In particular, As^{3+} ions in $AsCl_3$ solution diffuse from the back surface to the front interface through the GBs due to the high diffusion coefficient at GBs (D_0). This step would substantially reduce the diffusion barrier of group V ions and facilitate sequential diffusion from GBs into GIs. When the small As^{3+} ions substitute for the V_{Te} (Te^{2-} ionic radius 2.21 Å), the local lattice unit will be distorted and the strong electronegativity of As^{3+} will absorb the surrounding electrons to form large As^{3-} ions until the formation of the large acceptor As_{Te}^{-} (with an As^{3-} ionic radius of 2.22 Å), which can stabilize the CdSeTe lattice. The other advantage is that the As^{3+} ions exist naturally in $AsCl_3$ solution, indicating zero ionization energy is needed to form As^{3+}, unlike the Cd_3V_2 or V_2Te_3 compounds with their strong covalent bonds, supplying possibilities for a low-temperature doping process.

Additionally, the doping mechanism differs between group I (for example, Cu and Ag) and group V ions in CdTe. Cu doping in CdTe prefers a Te-rich (that is, Cd-poor) condition to promote Cu_{Cd} acceptor formation[37], while As in CdTe desires a Te-poor (that is, Cd-rich) condition to drive the As_{Te} acceptor formation[20]. Our ex situ group V diffusion doping is processed on the chlorinated CdSeTe. We have demonstrated previously that polycrystalline CdTe GBs become Te-poor after $CdCl_2$ treatment[38]. $CdCl_2$ treatment can compensate for some of the lost Cd in the GBs of as-deposited CdTe (Supplementary Fig. 5). Theoretically, the As_{Te} acceptor formation energy (1.2 eV) under Cd-rich conditions (GBs) is smaller than it is in the Cd-poor grain interior (1.9 eV) as shown in Supplementary Table 4 (ref. [39]). Thus, the defect chemistry in the chlorinated polycrystalline CdTe is favourable to the application of group V diffusion doping using $AsCl_3$. By contrast, other reported ex situ group V doping is accomplished by sealing Cd_3V_2 powder, extra Cd powder and CdTe stacks inside quartz ampoules and annealing at temperatures of 550–750 °C after $CdCl_2$ treatment, which may result in the loss of Cl and the reappearance of stacking faults[20,40]. Other in situ group V doping methods require an extra dopant activation process and $CdCl_2$ treatment after the group V doping in CdTe, which may deactivate the doped group V element by subsequent Cl processes[5].

Table 1 | *J–V* characteristics of CuCl and $AsCl_3$ doped CdSeTe devices

Dopants in CdSeTe	V_{OC} (mV)	J_{SC} (mA cm^{-2})	FF (%)	PCE (%)
CuCl	852	28.2	66.7	16.0
$AsCl_3$	863	28.9	72.1	18.0

Therefore, using the $AsCl_3$ as a dopant source can avoid the complex activation process and excess Cd vapour process, promising a higher potential for better device performance[7,14,39].

Performance of ex situ group V doped CdSeTe devices. Figure 3 shows the current density versus voltage (*J–V*) curves from the champion CdSeTe solar cells with ex situ doping by CuCl and $AsCl_3$. The performance of other group V chloride doped CdSeTe solar cells can be seen in Supplementary Fig. 6. The corresponding external quantum efficiency (EQE) curves are shown in Fig. 3b. Table 1 lists the device parameters for the *J–V* curves and the current density measured by integrated EQE. The low-temperature ex situ $AsCl_3$ doped polycrystalline CdSeTe solar cell without antireflection coating shows a PCE of ~18%. Figure 3c–f shows the statistical device parameters of the CuCl and $AsCl_3$ doped CdSeTe solar cells. The device performance statistics of ~300 CuCl and $AsCl_3$ doped cells are shown in Supplementary Fig. 7, indicating good repeatability for $AsCl_3$ doped devices.

The thermal diffusion conditions (diffusion temperature and diffusion time) and the $AsCl_3$ solution concentration highly impact the device performance (Supplementary Figs. 8 and 9). Remarkably, the $AsCl_3$ doped CdSeTe device performance is higher than that of the CuCl doped CdSeTe device. The best V_{OC} from the $AsCl_3$ doped CdSeTe devices can reach 863 mV, which is much higher than that of our best Cu doped CdSeTe devices (852 mV) and that of in situ Cd_3As_2 doped CdSeTe devices reported in the literature (856 mV), implying a low V_{OC} deficit of 537 mV (ref. [5]). To exclude the influence of unintentional Cu contamination, dynamic SIMS was used to investigate the Cu concentration in undoped, Cu doped and As doped CdSeTe devices (Supplementary Fig. 10). The Cu concentration in the Cu doped CdSeTe device is one order of magnitude higher in the bulk and three orders of magnitude higher at the back surface than the Cu concentrations in the undoped and As doped CdSeTe devices. Additionally, the device without any intentional Cu doping shows very poor performance, with an efficiency of 1.68%. Therefore, the unintentional Cu doping in the As doped CdSeTe device does not make a noticeable contribution to the high efficiency. CdSeTe devices are known to have high photocurrents due to the CdSe/CdTe interdiffusion forming a gradient CdSeTe alloy with a bandgap of ~1.4 eV after $CdCl_2$ treatment[6,41]. The gain in short-wavelength EQE response (300 to 400 nm) is likely due to the defect level at the front interface being shallower in the As doped device than in the Cu doped device, leading to less recombination centres or shunt pathways[42–44]. This is further confirmed by the admittance spectroscopy measurements described later.

Notably, the efficiency achieved with ex situ $AsCl_3$ diffusion doping is still lower than that of in situ Cd_3As_2 doped CdTe-based solar cells, mainly due to its relatively low fill factor of ~72.1% (compared to ~80% in in situ Cd_3As_2 doped CdSeTe cells using ZnTe back contact)[5]. The low FF of our As doped CdSeTe devices mainly originates from the high resistivity of the carbon electrode (~14 Ω sq^{-1}) and low quality of the CdSeTe/carbon interface (Supplementary Fig. 11). Higher FFs and efficiencies can be expected by replacing the carbon electrode with alternative back contacts to reduce the series resistivity and shunting for better carrier collection. An accelerated stress test under 1 sun and 85 °C light soaking conditions demonstrated that the As doped CdSeTe has better stability than the Cu doped devices (Supplementary Fig. 12). However, detailed insights into the stability of our low-temperature group V doped CdSeTe are beyond the scope of this work.

Improved hole lifetime and density. Figure 4a presents the carrier lifetimes of CuCl and $AsCl_3$ doped CdSeTe devices obtained from time-resolved photoluminescence (TRPL). The $AsCl_3$ doped CdSeTe devices show a longer mean minority carrier lifetime (22.0 ns) than the CuCl doped devices (16.3 ns), and one that is an order of magnitude higher than that of in situ doped polycrystal CdSeTe reported in the literature (Supplementary Table 1). Enhanced carrier lifetime in the As doped CdSeTe device is further demonstrated by the improved steady-state photoluminescence (PL) spectrum intensity measured from the glass side (Fig. 4b). The PL peak position at ~1.4 eV corresponds to the CdSeTe formed in the front[6]. Both the TRPL and PL results suggest reduced non-radiative recombination at the front interface. Meanwhile, Supplementary Fig. 13 illustrates the spatial variation of PL emission intensity in a cross-section of the As doped CdSeTe.

The hole density profiles of $AsCl_3$ doped and CuCl doped CdSeTe obtained from *C–V* measurements are shown in Fig. 4c. The hole densities corresponding to zero applied bias (N_A), also shown in Fig. 4c, are ~7.21×10^{14} cm^{-3} for the Cu doped cell and ~2.51×10^{15} cm^{-3} for the As doped cell. The results of the *C–V* measurement for other group V chloride doped devices can be seen in Supplementary Fig. 14. The hole densities in low-temperature ex situ doped CdSeTe (2.51×10^{15} cm^{-3}) are about two orders of magnitude lower than those in the high-temperature in situ doped polycrystalline CdSeTe (~1×10^{17} cm^{-3}) (ref. [5]) and high-temperature ex situ diffusion doped single-crystal CdTe (~1×10^{17} cm^{-3}) (ref. [4]). The low-temperature diffusion doping using $AsCl_3$ may lead to less group V dopants being incorporated into the CdSeTe bulk. The activation ratio of the As dopants in ex situ $AsCl_3$ doped CdSeTe film bulk is ~5.88%, as calculated by $N_{A,As}$/[As], where $N_{A,As}$ is hole density (~2.51×10^{15} cm^{-3}) at zero bias obtained from the *C–V* measurement and [As] is the average [As] (~4.27×10^{16} cm^{-3}) between the FTO/CdSeTe interface and ~2.0 μm away from it, as marked inside the back dashed square in Fig. 2c. With such a low-temperature $AsCl_3$ doping treatment, the activation ratio is higher than that with the high-temperature in situ As doped CdSeTe thin films (~1.5%) with a reduced V_{OC} of ~856 mV (ref. [5]). A high dopant activation ratio generally produces a higher V_{OC} as a result of the reduced density of the radiative recombination centres. Single-crystal CdTe solar cells doped with P using the ex situ method have demonstrated an activation ratio of ~50%, delivering an impressive V_{OC} exceeding 1 V (ref. [4]). It may be possible to further improve the device performance towards 25% using our low-temperature group V diffusion doping approach by exploring various activation procedures to activate more incorporated As in the CdSeTe devices with the goal of achieving an As doped CdSeTe absorber with a hole density >10^{16} cm^{-3}.

Thermal admittance spectroscopy (TAS) was performed to investigate the trap-state activation energies in the CuCl and $AsCl_3$ doped CdSeTe devices (Supplementary Fig. 15), and the Arrhenius plots of admittance spectroscopy signatures were extracted as shown in Fig. 4d. Two signatures in the CuCl doped CdSeTe can be observed in the TAS, as shown in Supplementary Fig. 15a, which is consistent with our previous results[45,46]. Surprisingly, in all the group V (As, Sb, Bi) doped devices, only one signature can be observed in the low-temperature range (Supplementary Fig. 15). It has been assigned as the back-barrier height between CdSeTe and metal back contact[45,46]. The CuCl doped devices show a back-barrier height $E_{b,Cu}=0.440$ eV, which is much higher than the $E_{b,As}=0.330$ eV in the $AsCl_3$ doped device. The back-barrier height calculated through the temperature-dependent *J–V* measurement (Supplementary Fig. 16)

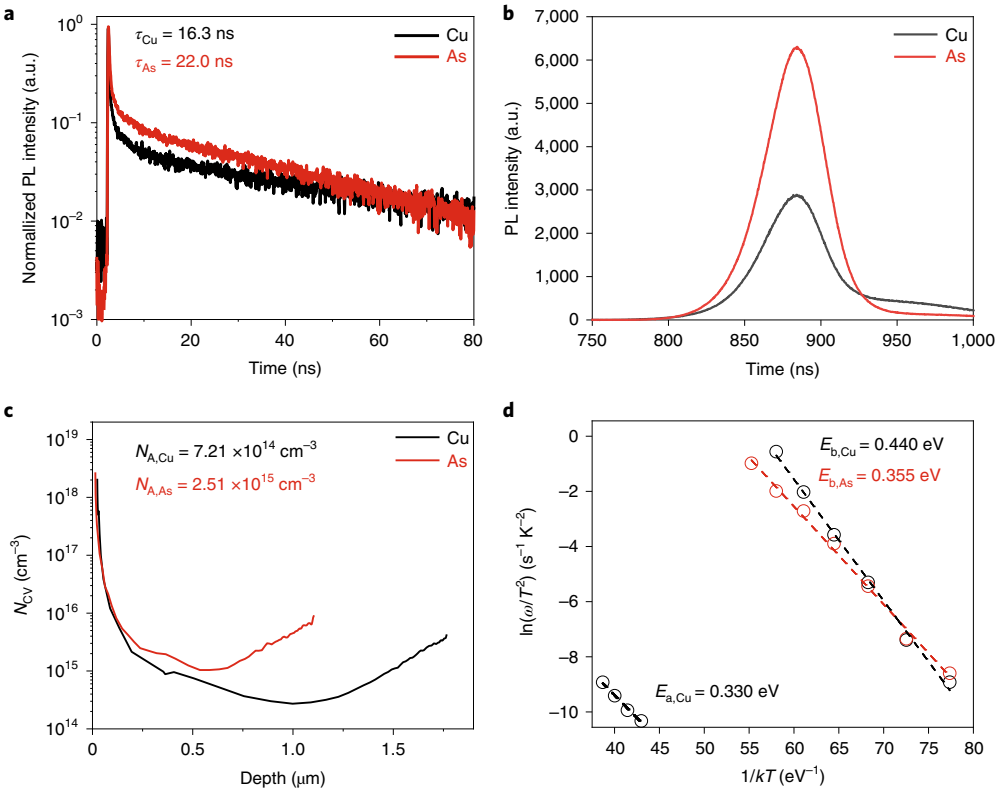

Fig. 4 | Absorber hole lifetime and hole densities. a, TRPL for Cu and As doped CdSeTe stacks. The carrier lifetimes of the Cu and As doped films (τ_{Cu} and τ_{As}, respectively) are shown in the top left. **b**, Steady-state PL curves for Cu and As doped CdSeTe stacks. Note that both TRPL and PL are measured using a 532 nm excitation laser excited from the glass side. **c**, Hole density profiles obtained from the capacitance–voltage (*C*–*V*) measurements (N_{CV}) for Cu and As doped CdSeTe devices. The hole density values were obtained at zero applied bias. **d**, The calculated defect activation energies *E* from the admittance spectroscopy measurements. The dashed lines show the linear fits used to extract the activation energies.

was 0.406 eV for the CuCl doped device and 0.298 eV for the $AsCl_3$ doped device, consistent with the values calculated from TAS measurements. The reduced back-barrier height further assists in better hole collection and, thus, higher FF and V_{OC}. The signature located at high temperature ($E_{a,Cu}$ = 0.330 eV) has been assigned as the defect activation energy of Cu_{Cd}^{+} (refs. [47,48]). The absence of defects related to As in CdTe could be due to the much lower activation energy of As_{Te} (~90 meV; Supplementary Table 4)[36,39].

Conclusions

We have demonstrated a low-temperature ex situ group V chloride diffusion doping to fabricate efficient Cu-free CdSeTe thin-film solar cells. Importantly, this low-temperature ex situ doping process produces an activation ratio as high as 5.88%, leading to both high hole density (on the order of 10^{15} cm^{-3}) and a long carrier lifetime (~22 ns). The best CdSeTe solar cell achieved a V_{OC} of 863 mV and an impressive PCE exceeding 18% through ex situ As doping, which is better than its Cu doped counterparts. Our approach paves a more effective pathway towards 25% efficiency and long-term stability through low-temperature group V diffusion doping in CdTe-based solar technology. More importantly, such a low-cost and low-temperature group V diffusion doping process is similar to the traditional Cu doping process and thus can be easily integrated with the manufacturing line, which can further make the CdTe-based solar cell technology more competitive in the solar market.

Methods

Computer simulations. All the calculations based on DFT are performed with gamma-point-only, semi-local Perdew–Burke–Ernzerhof (PBE) functional implemented in CP2K (refs. [49,50]). The basis set is double zeta valence polarization optimized on molecular geometries (shorter range)[51], and the energy cut-off is 600 Ry. We use a 4×4×4 CdTe supercell as the simulation model. The transition state searching is carried out using the nudged elastic band method. For the simulation of impurity atoms in defect systems, both V_{Cd} and V_{Te} were present in each of the models to ensure stoichiometry.

Materials. PCl_3 (99.998% purity, STREM Chemicals), $AsCl_3$ (99.999% purity, Alfa Aesar), $SbCl_3$ (99.999% purity, Alfa Aesar), $BiCl_3$ (99.997% purity, Alfa Aesar), $CdCl_2$ (99.99% purity, Alfa Aesar), CuCl (99.999% purity, Alfa Aesar), anhydrous isopropanol (99.9% purity, J. T. Baker), anhydrous acetone (99.5% purity, J. T. Baker), anhydrous benzene (99.8% purity, Sigma-Aldrich) and anhydrous methanol (99.8% purity, J. T. Baker) were commercial products. The solvent is of analytical purity grade and was used as received without further purification.

Deposition of CdSe/CdTe bilayer and solution-based $CdCl_2$ heat treatment. The ~110 nm CdSe film was deposited on cleaned FTO substrate coated with 30 nm tin oxide (TEC12D, NSG USA) by radiofrequency sputtering under a gas flow rate of 24 s.c.c.m. at 10 mtorr. Then ~3.5 μm CdTe film was deposited by closed space sublimation under a mixed gas flow rate of 1,500 s.c.c.m. Ar and 10 s.c.c.m. O_2 at 10 torr with a source temperature of 660 °C and a substrate temperature of ~600 °C (ref. [29]). The $CdCl_2$ heat treatment for the CdSeTe thin film was carried out at 400 °C for 30 min in a closed space sublimation chamber under a flow rate of 500 s.c.c.m. dry air at ambient pressure with $CdCl_2$ solution dropwise on the as-deposited CdSe/CdTe bilayer[52]. After cooling down, the CdSeTe surface was rinsed using deionized water to remove the residual $CdCl_2$ before undergoing an etching process using a dilute HCl solution to remove the surface oxide layer before further doping treatment.

Preparation of group V halide solution and CuCl solution for doping. The group V halides PCl_3, $AsCl_3$, $SbCl_3$, $BiCl_3$ and CuCl were dissolved in anhydrous benzene, isopropanol, acetone, methanol and ethanol, respectively, at concentrations of 1 to 100 mg l^{-1} based on the individual group V halide solubility (Supplementary Table 3). Note that these group V halides are easily hydrolysed and must be protected from moisture. $AsCl_3$ in particular is highly toxic and should be handled carefully in the glovebox. Here, all the group V halide solutions

were prepared in a N_2-filled glovebox with moisture and oxygen levels below than 1 p.p.m. The solutions were magnetically stirred at room temperature until fully dissolved.

Deposition of the group V and Cu halides on the CdSeTe surface. The group V chlorides (PCl_3, $AsCl_3$, $SbCl_3$ and $BiCl_3$) and CuCl solutions were applied directly to the CdSeTe surface by spin-coating with various solution concentrations (1–100 mgl^{-1}) at a spin-coating speed of 1,000 r.p.m. for 30 seconds. The samples were dried to form the group V chloride and CuCl layer on the CdSeTe surface. This process was performed in the N_2-filled glovebox (Supplementary Fig. 2).

Carbon back contact fabrication of CdSeTe device. The carbon back contact for the CdSeTe cells was doctor-bladed using a carbon paste and Ag paste without intentional Cu source, respectively, in a N_2-filled glovebox to prevent the hydrolysis of group V halides. The cell area is 0.08 cm^2.

Low-temperature diffusion doping of CdSeTe devices. For the solution-processed ex situ group V doping, after applying carbon electrode the ex situ group V chlorides and CuCl doped CdSeTe devices were heated to diffuse the group V and Cu ions into the CdSeTe absorber (details in Fig. 1 and Supplementary Fig. 2). The dopants were thermally activated for various durations (10–30 min) and at different temperatures (200–240 °C) to activate the group V and Cu dopants in the CdSeTe. The diffusion annealing conditions significantly impact device performance. The low-temperature ex situ diffusion doping process that yielded the highest device efficiencies in each case was identified over the course of the optimization of 400 devices.

Measurement of ex situ group V doped CdSeTe solar cell. The *J*–*V* curves of the solar cells were characterized from −0.5 V to 1.5 V bias in steps of 8 mV with a dwell time of 2 ms using a solar simulator (Newport, Oriel Class AAA 94063 A, 1,000 W xenon light source) with a source metre (Keithley 2420) at 100 mW cm^{-2} AM 1.5G irradiation. A calibrated Si reference cell and metre (Newport, 91150 V, certificated by NREL) were used to calibrate the solar simulator prior to cell measurements. More than 400 cells were tested with various ex situ doping. EQE data were characterized by a solar cell spectral response measurement system (QE-T, Enli Technology, Co. Ltd). The *C*–*V* and TAS measurements were performed using a Solartron Modulab potentiostat equipped with a frequency response analyser (Ametek Inc.). The *C*–*V* measurements were performed in the dark with a constant 45 mV r.m.s. 10 kHz AC signal superimposed on a DC bias voltage varying from 2.5 to 0.5 V. All *J*–*V*, EQE and *C*–*V* measurements were performed at room temperature in air. The TAS measurements were performed with frequencies varying from 1.0 MHz to 0.1 Hz and DC bias sweeping from −0.3 V to 0.2 V with an interval of 0.1 V. A liquid nitrogen cooling cryo-system (Janis VPF-100 system) was used to carry out all the temperature-dependent (150 to 300 K with a step size of 10 K) measurements. The temperature was controlled by a temperature controller (Lakeshore 330). A sensor was mounted directly on the top of the device to ensure that the recorded temperature was the device temperature. PL characteristics for all devices were investigated using steady-state PL and TRPL. PL measurements were performed using a 532 nm continuous-wave laser at ~5 W cm^{-2} excited through the FTO side. The PL signal was detected by liquid nitrogen-cooled symphony-II Si CCD (charge-coupled device) detector after a Horiba iHR320 monochromator. The TRPL measurements of CdTe samples were performed with a 532 nm pulsed laser whose photon fluence is 1.2×10^{11} photons cm^{-2} $pulse^{-1}$ with a repetition rate of 10 MHz when the samples were excited through the FTO side at the peak emission wavelength of 885 nm as determined from the PL measurement. The TRPL measurements of CdSeTe samples were performed with time-correlated single photon counting module with integration time 600 s bi-exponential PL decays. A Horiba iHR320 monochromator was used to select the detection wavelength using a hybrid detector from Becker & Hickl. The cross-sectional PL mapping for the CdSeTe device was performed using a Klar microscope (Klar Scientific). The accelerated stress test was performed at 1 sun and 85 °C in a light soaking stage.

Characterization of the ex situ group V doped CdSeTe device. XPS was conducted in a Kratos Axis Ultra DLD system equipped with a monochromatic Al X-ray source and a 5 keV Ar-ion sputter gun for depth profiling of samples. The base pressure in the analysis chamber was $<8 \times 10^{-10}$ torr. Scanning electron microscopy (SEM) was carried out in a Thermo Scientific Apreo field-emission SEM (FE-SEM) equipped with X-ray dispersive energy spectroscopy. The dynamic SIMS analyses were performed on a Cameca IMF-6f (810 Kifer Road, Sunnyvale, CA) double-focusing magnetic sector instrument. The samples were bombarded by a focused Cs^+ primary ion beam with a net impact energy of 5 keV and about 100 nA of beam current. The beam is rastered over a square area of 200 μm on a side. The secondary ions formed from the sputtering process are accelerated away from the sample surface by a nominal sample voltage of 5 kV. A fraction of secondary ions is collected from a circular region centred in the rastered area.

Reporting Summary. Further information on research design is available in the Nature Research Reporting Summary linked to this article.

Data availability

All data generated or analysed during this study are included in the published article and its Supplementary Information. Source data are provided with this paper.

Received: 14 October 2020; Accepted: 26 April 2021;
Published online: 24 June 2021

References

1. Green, M. A. et al. Solar cell efficiency tables (version 54). *Prog. Photovolt. Res. Appl.* **27**, 565–575 (2019).
2. Grover, S. et al. Characterization of arsenic doped CdTe layers and solar cells. In *Proc. 2017 IEEE 44th Photovoltaic Specialist Conference (PVSC)* 1193–1195 (IEEE, 2017).
3. *Leading the World's Sustainable Energy Future* (First Solar, 2019); http://www.firstsolar.com/-/media/First-Solar/Documents/Corporate-Collaterals/FS_Corporate_Factsheet.ashx
4. Burst, J. M. et al. CdTe solar cells with open-circuit voltage breaking the 1 V barrier. *Nat. Energy* **1**, 16015 (2016).
5. Metzger, W. K. et al. Exceeding 20% efficiency with in situ group V doping in polycrystalline CdTe solar cells. *Nat. Energy* **4**, 837–845 (2019).
6. Fiducia, T. A. M. et al. Understanding the role of selenium in defect passivation for highly efficient selenium-alloyed cadmium telluride solar cells. *Nat. Energy* **4**, 504–511 (2019).
7. McCandless, B. E. et al. Overcoming carrier concentration limits in polycrystalline CdTe thin films with in situ doping. *Sci. Rep.* **8**, 14519 (2018).
8. Dzhafarov, T. D., Yesilkaya, S. S., Yilmaz Canli, N. & Caliskan, M. Diffusion and influence of Cu on properties of CdTe thin films and CdTe/CdS cells. *Sol. Energy Mater. Sol. Cells* **85**, 371–383 (2005).
9. Yang, J. H., Yin, W. J., Park, J. S., Ma, J. & Wei, S. H. Review on first-principles study of defect properties of CdTe as a solar cell absorber. *Semicond. Sci. Tech.* **31**, 083002 (2016).
10. Ma, J. et al. Dependence of the minority-carrier lifetime on the stoichiometry of CdTe using time-resolved photoluminescence and first-principles calculations. *Phys. Rev. Lett.* **111**, 067402 (2013).
11. Nagaoka, A. et al. Growth and characterization of arsenic doped CdTe single crystals grown by Cd-solvent traveling-heater method. *J. Cryst. Growth* **467**, 6–11 (2017).
12. Kartopu, G. et al. Study of thin film poly-crystalline CdTe solar cells presenting high acceptor concentrations achieved by in-situ arsenic doping. *Sol. Energy Mater. Sol. Cells* **194**, 259–267 (2019).
13. Ghandhi, S. K., Taskar, N. R. & Bhat, I. B. Arsenic-doped P-CdTe layers grown by organometallic vapor-phase epitaxy. *Appl. Phys. Lett.* **50**, 900–902 (1987).
14. Nagaoka, A., Nishioka, K., Yoshino, K., Kuciauskas, D. & Scarpulla, M. A. Arsenic doped Cd-rich CdTe: equilibrium doping limit and long lifetime for high open-circuit voltage solar cells greater than 900 mV. *Appl. Phys. Express* **12**, 081002 (2019).
15. Krasikov, D. & Sankin, I. Beyond thermodynamic defect models: a kinetic simulation of arsenic activation in CdTe. *Phys. Rev. Mater.* **2**, 103803 (2018).
16. Li, D.-B. et al. Maximize CdTe solar cell performance through copper activation engineering. *Nano Energy* **73**, 104835 (2020).
17. Artegiani, E. et al. Analysis of a novel $CuCl_2$ back contact process for improved stability in CdTe solar cells. *Prog. Photovolt. Res. Appl.* **27**, 706–715 (2019).
18. Mao, D., Wickersham, C. E. & Gloeckler, M. Measurement of chlorine concentrations at CdTe grain boundaries. *IEEE J. Photovolt.* **4**, 1655–1658 (2014).
19. Colegrove, E. et al. Phosphorus diffusion mechanisms and deep incorporation in polycrystalline and single-crystalline CdTe. *Phys. Rev. Appl.* **5**, 054014 (2016).
20. Colegrove, E. et al. Experimental and theoretical comparison of Sb, As, and P diffusion mechanisms and doping in CdTe. *J. Phys. D Appl. Phys.* **51**, 075102 (2018).
21. Kraft, C. et al. Phosphorus implanted cadmium telluride solar cells. *Thin Solid Films* **519**, 7153–7155 (2011).
22. Romeo, N., Bosio, A. & Rosa, G. The back contact of CdTe/CdS thin film solar cells. In *Proc. ISES Solar World Congress 2017* (International Solar Energy Society Selection, 2017).
23. Hu, S. et al. Band diagrams and performance of CdTe solar cells with a Sb_2Te_3 back contact buffer layer. *AIP Adv.* **1**, 042152 (2011).
24. Kumar, S. G. & Rao, K. S. R. K. Physics and chemistry of CdTe/CdS thin film heterojunction photovoltaic devices: fundamental and critical aspects. *Energy Environ. Sci.* **7**, 45–102 (2014).
25. Huang, J. et al. Copassivation of polycrystalline CdTe absorber by CuCl thin films for CdTe solar cells. *Appl. Surf. Sci.* **484**, 1214–1222 (2019).
26. Bastola, E. et al. Doping of CdTe using CuCl2 solution for highly efficient photovoltaic devices. In *Proc. 2019 IEEE 46th Photovoltaic Specialists Conference (PVSC)* 1846–1850 (IEEE, 2019).

27. Major, J. D., Treharne, R. E., Phillips, L. J. & Durose, K. A low-cost non-toxic post-growth activation step for CdTe solar cells. *Nature* **511**, 334–337 (2014).
28. Abbas, A. et al. The effect of a post-activation annealing treatment on thin film CdTe device performance. In *Proc. 2015 IEEE 42nd Photovoltaic Specialist Conference (PVSC)* 1–6 (IEEE, 2015).
29. Montgomery, A. et al. Solution-processed copper (I) thiocyanate (CuSCN) for highly efficient CdSe/CdTe thin-film solar cells. *Prog. Photovolt. Res. Appl.* **27**, 665–672 (2019).
30. Fiducia, T. et al. 3D distributions of chlorine and sulphur impurities in a thin-film cadmium telluride solar cell. *MRS Adv.* **3**, 3287–3292 (2018).
31. Akis, R. et al. Extracting Cu diffusion parameters in polycrystalline CdTe. In *Proc. 2014 IEEE 40th Photovoltaic Specialist Conference (PVSC)* 3276–3281 (IEEE, 2014).
32. Colegrove, E. et al. Antimony diffusion in CdTe. *IEEE J. Photovolt.* **7**, 870–873 (2017).
33. Flores, M. A., Orellana, W. & Menéndez-Proupin, E. Self-compensation in phosphorus-doped CdTe. *Phys. Rev. B* **96**, 134115 (2017).
34. Barrioz, V. et al. Highly arsenic doped CdTe layers for the back contacts of CdTe solar cells. *MRS Proc.* **1012**, 1208 (2007).
35. Murria, P. et al. Speciation of CuCl and $CuCl_2$ thiol-amine solutions and characterization of resulting films: implications for semiconductor device fabrication. *Inorg. Chem.* **56**, 14396–14407 (2017).
36. Molva, E., Saminadayar, K., Pautrat, J. L. & Ligeon, E. Photoluminescence studies in N, P, As implanted cadmium telluride. *Solid State Commun.* **48**, 955–960 (1983).
37. Yun, J. H., Kim, K. H., Lee, D. Y. & Ahn, B. T. Back contact formation using Cu_2Te as a Cu-doping source and as an electrode in CdTe solar cells. *Sol. Energy Mater. Sol. Cells* **75**, 203–210 (2003).
38. Li, C. et al. Grain-boundary-enhanced carrier collection in CdTe solar cells. *Phys. Rev. Lett.* **112**, 156103 (2014).
39. Ablekim, T. et al. Self-compensation in arsenic doping of CdTe. *Sci. Rep.* **7**, 4563 (2017).
40. Guo, J. L. et al. Effect of selenium and chlorine co-passivation in polycrystalline CdSeTe devices. *Appl. Phys. Lett.* **115**, 153901 (2019).
41. Poplawsky, J. D. et al. Structural and compositional dependence of the $CdTe_xSe_{1-x}$ alloy layer photoactivity in CdTe-based solar cells. *Nat. Commun.* **7**, 12537 (2016).
42. Grecu, D. & Compaan, A. D. Photoluminescence study of Cu diffusion and electromigration in CdTe. *Appl. Phys. Lett.* **75**, 361–363 (1999).
43. Corwine, C. R., Pudov, A. O., Gloeckler, M., Demtsu, S. H. & Sites, J. R. Copper inclusion and migration from the back contact in CdTe solar cells. *Sol. Energy Mater. Sol. Cells* **82**, 481–489 (2004).
44. Dobson, K. D., Visoly-Fisher, I., Hodes, G. & Cahen, D. Stability of CdTe/CdS thin-film solar cells. *Sol. Energy Mater. Sol. Cells* **62**, 295–325 (2000).
45. Awni, R. A. et al. The effects of hydrogen iodide back surface treatment on CdTe solar cells. *Sol. RRL* **3**, 1800304 (2019).
46. Awni, R. A. et al. Influences of buffer material and fabrication atmosphere on the electrical properties of CdTe solar cells. *Prog. Photovolt. Res. Appl.* **27**, 1115–1123 (2019).
47. Perrenoud, J. et al. A comprehensive picture of Cu doping in CdTe solar cells. *J. Appl. Phys.* **114**, 174505 (2013).
48. Wei, S.-H. & Zhang, S. B. Chemical trends of defect formation and doping limit in II-VI semiconductors: the case of CdTe. *Phys. Rev. B* **66**, 155211 (2002).
49. Perdew, J. P., Burke, K. & Ernzerhof, M. Generalized gradient approximation made simple. *Phys. Rev. Lett.* **77**, 3865–3868 (1996).
50. Hutter, J., Iannuzzi, M., Schiffmann, F. & VandeVondele, J. cp2k: atomistic simulations of condensed matter systems. *Wiley Interdiscip. Rev. Comput. Mol. Sci.* **4**, 15–25 (2014).
51. VandeVondele, J. & Hutter, J. Gaussian basis sets for accurate calculations on molecular systems in gas and condensed phases. *J. Chem. Phys.* **127**, 114105 (2007).
52. Li, D.-B. et al. Eliminating S-kink to maximize the performance of MgZnO/CdTe solar cells. *ACS Appl. Energy Mater.* **2**, 2896–2903 (2019).

Acknowledgements

S.N.V., L.L. and F.Y. acknowledge funding from the National Science Foundation under contracts no. 1944374 and 2019473, the National Aeronautics and Space Administration, Alabama EPSCoR International Space Station Flight Opportunity Program (contract no. 80NSSC20M0141) and the US Department of Energy's Office of Energy Efficiency and Renewable Energy (EERE) under the Solar Energy Technologies Office (SETO) Agreement DE-EE0009368. D.-B.L., C.Y., R.A.A., K.K.S., R.J.E. and Y.Y. acknowledge funding from the Air Force Research Laboratory, Space Vehicles Directorate (contract no. FA9453-18-2-0037), the National Science Foundation under contract no. 1711534 and the US Department of Energy's Office of Energy Efficiency and Renewable Energy (EERE) under Solar Energy Technologies Office (SETO) Agreement DE-EE0008974. We thank D. Strickler from Pilkington North America Inc. for supplying us with the FTO coated substrates.

Author contributions

D.-B.L. and S.N.V. performed film and device synthesis as well as *J–V*, EQE and *C–V* measurements. S.N.V. performed the XPS measurements. C.Y. performed the DFT calculations. R.A.A. carried out TAS and temperature-dependent *J–V* measurements. K.K.S. and R.J.E. performed the PL and TRPL measurements. L.L. performed the PL mapping. Y.Y. and F.Y. directed the research.

Competing interests

The authors declare no competing interests.

Additional information

Supplementary information The online version contains supplementary material available at https://doi.org/10.1038/s41560-021-00848-z.

Correspondence and requests for materials should be addressed to Y.Y. or F.Y.

Peer review information *Nature Energy* thanks Gang Xiong and the other, anonymous, reviewer(s) for their contribution to the peer review of this work.

Reprints and permissions information is available at www.nature.com/reprints.

Publisher's note Springer Nature remains neutral with regard to jurisdictional claims in published maps and institutional affiliations.

nature research

Corresponding author(s): Yanfa Yan, Feng Yan

Solar Cells Reporting Summary

Nature Research wishes to improve the reproducibility of the work that we publish. This form is intended for publication with all accepted papers reporting the characterization of photovoltaic devices and provides structure for consistency and transparency in reporting. Some list items might not apply to an individual manuscript, but all fields must be completed for clarity.

For further information on Nature Research policies, including our data availability policy, see Authors & Referees.

Experimental design

Please check: are the following details reported in the manuscript?

1. Dimensions

Area of the tested solar cells	☒ Yes	Methods - Carbon back contact fabrication of CdSeTe device. Cells area of 0.08 cm2
	☐ No	*Explain why this information is not reported/not relevant.*
Method used to determine the device area	☒ Yes	Methods - Carbon back contact fabrication of CdSeTe device. The active area was determined by the mask used for the carbon electrode.
	☐ No	*Explain why this information is not reported/not relevant.*

2. Current-voltage characterization

Current density-voltage (J-V) plots in both forward and backward direction	☐ Yes	*State where this information can be found in the text.*
	☒ No	Hysteresis is not oberved
Voltage scan conditions *For instance: scan direction, speed, dwell times*	☒ Yes	Methods - Measurement of ex-situ Group V doped CdSeTe solar cell. From -0.5 V to 1.5 V bias in steps of 8mV, with a dwell time of 2ms
	☐ No	*Explain why this information is not reported/not relevant.*
Test environment *For instance: characterization temperature, in air or in glove box*	☒ Yes	Methods - Measurement of ex-situ Group V doped CdSeTe solar cell. The cells were measured at room temperature in air.
	☐ No	*Explain why this information is not reported/not relevant.*
Protocol for preconditioning of the device before its characterization	☐ Yes	*State where this information can be found in the text.*
	☒ No	No preconditioning is required for our characterization.
Stability of the J-V characteristic *Verified with time evolution of the maximum power point or with the photocurrent at maximum power point; see ref. 7 for details.*	☒ Yes	Supplementary Fig. 12 Short term accelerated stress test of our devices without encapsulation under AM1.5 illumination, 85 oC in ambient air has been performed and the As doped devices show higher stability properties than Cu doped devices
	☐ No	Not an issue for CdSeTe Solar Cell

3. Hysteresis or any other unusual behaviour

Description of the unusual behaviour observed during the characterization	☐ Yes	*State where this information can be found in the text.*
	☒ No	Hysteresis is not observed.
Related experimental data	☐ Yes	*State where this information can be found in the text.*
	☒ No	Hysteresis is not observed.

4. Efficiency

External quantum efficiency (EQE) or incident photons to current efficiency (IPCE)	☒ Yes	Figure 3b and methods
	☐ No	*Explain why this information is not reported/not relevant.*
A comparison between the integrated response under the standard reference spectrum and the response measure under the simulator	☒ Yes	Methods
	☐ No	*Explain why this information is not reported/not relevant.*
For tandem solar cells, the bias illumination and bias voltage used for each subcell	☐ Yes	*State where this information can be found in the text.*
	☒ No	These are not tandem cells

5. Calibration

Light source and reference cell or sensor used for the characterization	☒ Yes ☐ No	Methods - Measurement of ex-situ Group V doped CdSeTe solar cell. The light intensity for J–V measurements was calibrated by a standard silicon wafer solar cell certified by Newport. A standard silicon wafer solar cell was used as the reference for the EQE measurement. *Explain why this information is not reported/not relevant.*
Confirmation that the reference cell was calibrated and certified	☒ Yes ☐ No	Methods - Measurement of ex-situ Group V doped CdSeTe solar cell. The light intensity for J–V measurements was calibrated by a standard silicon wafer solar cell certified by Newport. A standard silicon wafer solar cell was used as the reference for the EQE measurement. *Explain why this information is not reported/not relevant.*
Calculation of spectral mismatch between the reference cell and the devices under test	☒ Yes ☐ No	Methods - Measurement of ex-situ Group V doped CdSeTe solar cell. A standard silicon wafer solar cell was used as the reference for the EQE measurement. *Explain why this information is not reported/not relevant.*

6. Mask/aperture

Size of the mask/aperture used during testing	☐ Yes ☒ No	*State where this information can be found in the text.* the carbon electrode area pretty thick (~18 um) and the cells area was measured directly
Variation of the measured short-circuit current density with the mask/aperture area	☐ Yes ☒ No	*State where this information can be found in the text.* *Explain why this information is not reported/not relevant.*

7. Performance certification

Identity of the independent certification laboratory that confirmed the photovoltaic performance	☐ Yes ☒ No	*State where this information can be found in the text.* Two corresponding groups cross check the device performance.The light intensity of our solar simulator for J-V and EQE measurement was calibrated by a standard silicon wafer solar cell
A copy of any certificate(s) *Provide in Supplementary Information*	☐ Yes ☒ No	*State where this information can be found in the text.* The light intensity of our solar simulator for J-V and EQE measurement was calibrated by a standard silicon wafer solar cell (Newport, 91150V, certificated by NREL)

8. Statistics

Number of solar cells tested	☒ Yes ☐ No	Methods - Measurement of ex-situ Group V doped CdSeTe solar cell. More than 300 cells have been tested with various ex-situ doping. *Explain why this information is not reported/not relevant.*
Statistical analysis of the device performance	☒ Yes ☐ No	Fig.3c-f. and Supplementary Fig.6c-f and Supplementary Fig.7 *Explain why this information is not reported/not relevant.*

9. Long-term stability analysis

Type of analysis, bias conditions and environmental conditions *For instance: illumination type, temperature, atmosphere humidity, encapsulation method, preconditioning temperature*	☒ Yes ☐ No	Supplementary Fig. 12 Short term accelerated stress test of our devices without encapsulation under AM1.5 illumination, 85 oC in ambient air has been performed and the As doped devices show higher stability properties than Cu doped devices. Long term stability testing is beyond the scope of this article. We will work on the long term stability test in the future.